University of Wollongong
Research Online

Faculty of Engineering - Papers (Archive)

Faculty of Engineering and Information Sciences

2012

Hydrogen De-/absorption improvement of NaBH4 catalyzed by titanium-based additives

Jianfeng Mao
University of Wollongong, jm975@uowmail.edu.au

Zaiping Guo
University of Wollongong, zguo@uow.edu.au

Ivan P. Nevirkovets
University of Wollongong, ivann@uow.edu.au

Hua-Kun Liu
University of Wollongong, hua@uow.edu.au

S. X. Dou
University of Wollongong, shi@uow.edu.au

Follow this and additional works at: https://ro.uow.edu.au/engpapers

 Part of the Engineering Commons

https://ro.uow.edu.au/engpapers/5222

Recommended Citation

Mao, Jianfeng; Guo, Zaiping; Nevirkovets, Ivan P.; Liu, Hua-Kun; and Dou, S. X.: Hydrogen De-/absorption improvement of NaBH4 catalyzed by titanium-based additives 2012, 1596-1604.
https://ro.uow.edu.au/engpapers/5222

Research Online is the open access institutional repository for the University of Wollongong. For further information contact the UOW Library: research-pubs@uow.edu.au

THE JOURNAL OF PHYSICAL CHEMISTRY C

ARTICLE

pubs.acs.org/JPCC

Hydrogen De-/Absorption Improvement of $NaBH_4$ Catalyzed by Titanium-Based Additives

Jianfeng Mao,*[,†] Zaiping Guo,*[,†,‡] Ivan P. Nevirkovets,[†] Hua Kun Liu,[†] and Shi Xue Dou[†]

[†]Institute for Superconducting and Electronic Materials, and [‡]School of Mechanical, Materials & Mechatronics Engineering, University of Wollongong, NSW 2522, Australia

Supporting Information

ABSTRACT: $NaBH_4$ is considered as a promising candidate material for solid-state hydrogen storage due to its high hydrogen content of 10.6 wt %. However, its practical use is hampered by its high thermodynamic stability and slow H-exchange kinetics. In the present work, the effects of Ti-based additives, including Ti, TiH_2, and TiF_3, on the dehydrogenation and rehydrogenation of $NaBH_4$ (NaH+B) were investigated. It was revealed that all of the titanium-based additives were effective in improving the hydrogen desorption and absorption reactions of $NaBH_4$, and, among them, TiF_3 possessed the highest catalytic activity. The whole dehydrogenation process for the $NaBH_4$−0.05TiF_3 sample can be regarded as a two-step process: (i) a preferential reaction ($3NaBH_4 + TiF_3 \rightarrow 3NaF + TiB_2 + B + 6H_2$) occurring at around 300 °C, and (ii) the formation of Ti- and F-containing species catalyze the dehydrogenation of the remaining $NaBH_4$. It was also indicated that the F anion can substitute for anionic H in NaH to form $NaF_{1-x}H_x$ in the case of NaH−B−0.05TiF_3 during the hydrogenation process. Therefore, the observed promotion effect of TiF_3 on the reversible dehydrogenation of $NaBH_4$ should be understood as arising from the combined effects of active Ti- and F-containing species. Also, FTIR spectroscopy confirmed the presence of amorphous $Na_2B_{12}H_{12}$, in both the dehydrogenated and the rehydrogenated states, which may play a role in the partial dehydrogenation and reversibility observed in $NaBH_4$ with and without catalyst doping.

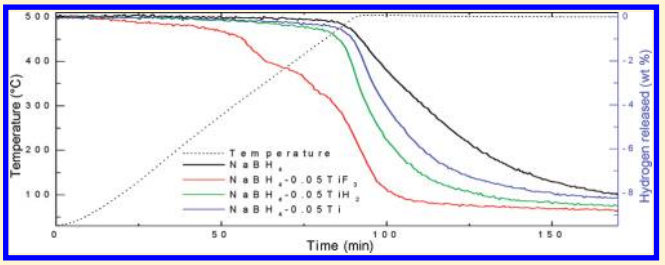

1. INTRODUCTION

Hydrogen is regarded as one of the best alternative energy carriers of sustainable energy because of its abundance, high energy density, and environmental friendliness. However, an important challenge to the use of hydrogen for mobile and small-scale energy generation is how to achieve compact, safe, and high density hydrogen storage.[1] As compared to pressurized cylinders and cryogenic liquid hydrogen, solid-state hydrogen storage in metal hydrides is now considered as a better way to handle hydrogen for on-board hydrogen storage due to its advantages in terms of safety and volumetric hydrogen density.[2] For automotive applications, a system target of 5.5 wt % H_2 capacity by 2015 has been set by the U.S. Department of Energy (DOE).[3] Light metal borohydrides such as $NaBH_4$,[4−6] $LiBH_4$,[7−14] $Mg(BH_4)_2$,[15,16] and $Ca(BH_4)_2$[17−19] have attracted much attention as potential hydrogen storage media due to their high volumetric and gravimetric capacities.

As the first known borohydride, $NaBH_4$ is relatively stable in air and has been widely used as a reducing agent in industrial and laboratory application. On the other hand, $NaBH_4$ has a high potential to be used as a hydrogen storage material due to its large gravimetric and volumetric hydrogen contents of 10.6 wt % and 113 kg of H_2 m^{-3} respectively.[20] Like many other metal hydrides, $NaBH_4$ can release hydrogen via hydrolysis or thermolysis. For hydrolysis, after doping with effective catalysts, $NaBH_4$ can react with water to yield hydrogen according to the following reaction:[21−23]

$$NaBH_4 + 2H_2O \rightarrow NaBO_2 + 4H_2 \quad (1)$$

Reaction 1 is the ideal and stoichiometric reaction; that is, 1 mol of $NaBH_4$ requires only 2 mol of H_2O. However, under real conditions, the reaction needs more water to release 4 mol of hydrogen and can be written as:

$$NaBH_4 + (2 + x)H_2O \rightarrow NaBO_2 \cdot xH_2O + 4H_2 \quad (2)$$

Therefore, the gravimetric hydrogen storage capacity (GHSC) of real storage systems will invariably be lower than the theoretical 10.6 wt %, due to the excess water required to dissolve the $NaBH_4$ and its byproduct, $NaBO_2$, as well as the added mass of the reaction and storage vessels. Hence, the DOE issued a "No-Go" recommendation for the hydrolysis of $NaBH_4$ in 2007, and since then, the hydrolysis of $NaBH_4$ has not been considered for the automotive applications.[24]

An alternative method to utilize the high hydrogen capacity of $NaBH_4$ is by thermal decomposition. However, as with other borohydrides,[7−19] the use of $NaBH_4$ for hydrogen storage is challenging because of both kinetic and thermodynamic limitations, due to the strong covalent and ionic bonds involved. For

Received: October 28, 2011
Revised: December 5, 2011
Published: December 07, 2011

ACS Publications © 2011 American Chemical Society

example, the complete dehydrogenation of $NaBH_4$ yields 10.6 wt % hydrogen according to the following reaction (without mentioning the possible intermediate phases NaH and $Na_2B_{12}H_{12}$).[25−27]

$$NaBH_4 \rightarrow Na + B + 2H_2 \quad (3)$$

The decomposition temperature of this reaction at 1 bar of H_2 is above 500 °C,[5] which is too high for practical application in hydrogen fuel cell vehicles.

Demonstrating cyclability and improved desorption are crucial in establishing $NaBH_4$ as a practical solution for on-board hydrogen storage. Recently, several novel strategies such as destabilization and nanosizing/nanoconfinement have been employed to address the thermodynamic and kinetic limitations of $NaBH_4$. For example, reversible reactions have been obtained for reactive hydride composites (RHC) such as $NaBH_4-MgH_2$,[28−35] $NaBH_4-LiAlH_4$,[36] and $NaBH_4-CaH_2$ ($Ca(BH_4)_2$),[37] which shows lower reaction enthalpy as compared to bare $NaBH_4$. Indeed, when $NaBH_4$ is combined with MgH_2, $LiAlH_4$, or CaH_2 ($Ca(BH_4)_2$), the borides MgB_2, AlB_2, and CaB_6 will be generated upon dehydrogenation, respectively, which stabilizes the dehydrogenated state of boron and, therefore, destabilizes the $NaBH_4$. Moreover, the formation of borides also allows the rehydrogenation reaction to take place under more moderate conditions, as the activation energy needed to break the B−M bond (where M is a metal) is significantly lower than that needed for the B−B bond.[38] On the other hand, nanosizing and confinement of $NaBH_4$ in porous carbon have also resulted in much faster hydrogen desorption kinetics.[27,39] However, the weight of the supporting substrate will reduce the total hydrogen storage capacity.

Another possible way to promote the hydrogen exchange reactions in $NaBH_4$ under moderate temperature and pressure conditions is the use of selected catalysts. It is well-known that transition metal-based compounds show catalytic activity in metal or complex hydrides. For example, Ti-based catalysts were the first group discovered as effective dopants for catalyzing $NaAlH_4$ to enable much lower hydrogen release temperatures, as well as imparting previously unattainable reversibility.[40] In particular, titanium compounds have been shown to be active in promoting the hydrogen desorption and absorption of borohydrides such as $LiBH_4$,[14] $Mg(BH_4)_2$,[15,16] and $Ca(BH_4)_2$[18] under moderate conditions. Furthermore, the H^-/F^- substitution in $NaAlH_4$[41,42] or $LiBH_4$[43,44] has been shown to positively tune the thermodynamics because the two anions are isostructural. However, a comprehensive study of the sorption and structural properties of $NaBH_4$ with additives has not been presented so far.

In this work, small amounts of titanium additives, including Ti, TiH_2, and TiF_3, were doped into $NaBH_4$ (NaH+B) to facilitate hydrogen release and potentially improve reversibility. A series of hydrogen release and uptake experiments have been designed to investigate the hydrogen storage properties of $NaBH_4$ with additives. It was found that TiF_3 exhibited the best catalytic efficiency toward enhancing dehydrogenation kinetics. X-ray diffraction (XRD), Fourier transform infrared spectroscopy (FTIR), and X-ray photoelectron spectroscopy (XPS) were employed to further characterize the roles of the products and additives during hydrogen release and absorption. The results showed that both Ti and F may play important roles in the improvement of the hydrogen storage performance of TiF_3-added $NaBH_4$, indicating that using metal fluorides as additives is a promising direction for improving the sorption kinetics of $NaBH_4$ by lowering the energy barriers for practical applications. We herein report the experimental results on $NaBH_4$ samples with and without titanium additives, as well as discuss the reaction and catalytic mechanism.

2. EXPERIMENTAL PROCEDURES

The chemicals $NaBH_4$ (98% purity), NaH (98% purity), B (95−97% purity), Ti (99.7% purity), TiH_2 (98% purity), and TiF_3 (99.99% purity) were all purchased from Sigma-Aldrich Corp. and used directly without pretreatment. All sample storage and handling was performed in an Ar-filled glovebox (MBraun Unilab). A QM-3SP2 planetary ball mill was employed to prepare the pristine $NaBH_4$, $NaBH_4-0.05TiF_3$, $NaBH_4-0.05TiH_2$, $NaBH_4-0.05Ti$, $3NaBH_4-TiF_3$, NaH−B, NaH−B−$0.05TiF_3$, NaH−B−$0.05TiH_2$, and NaH−B−0.05Ti samples (all in molar ratio) under an argon atmosphere at 400 rpm. Each time, about 1 g of sample was prepared with 2 h of ball milling, with a ball-to-powder ratio of around 30:1. The hydrogen desorption/absorption properties were measured in a Sieverts apparatus (Advanced Materials Corp., U.S.), where the temperatures and pressures of the sample and the gas reservoirs were monitored and recorded by GrcLV-LabVIEW-based control program software during the sorption process. Temperature-programmed desorption (TPD) curves were determined by volumetric methods, starting from static vacuum. The temperature was increased from ambient to ∼500 °C at a 5 °C/min heating rate. The isothermal hydrogen desorption measurements were performed at 440 °C, starting from static vacuum. Before the measurement, the sample chamber was filled with hydrogen at 5.5 MPa pressure, and the temperature was then quickly raised to and kept at the desired temperature. Next, the chamber was quickly evacuated before the onset of measurements. The hydrogen absorption measurements were performed under ∼5.5 MPa hydrogen pressure at 500 °C. To evaluate the practical hydrogen storage properties, the weight percent of hydrogen released and uptaked for the sample with additives was calculated on the basis of the total weight of the samples.

The phase structures of various samples after ball milling and the milled samples after dehydrogenation and rehydrogenation were identified by a GBC X-ray diffractometer (XRD) with Cu Kα radiation at 40 kV and 25 mA. To avoid oxidation during the XRD measurement, samples were mounted on a glass slide 1 mm in thickness in the Ar-filled glovebox and sealed with an airtight hood composed of polyvinyl chloride (PVC) tape. The obtained samples were ground with KBr and pressed into a sample cup, and the vibration spectra of the species were then identified using a Shimadzu Prestige 21 Fourier transform infrared spectrometer (FTIR) in transmission mode. X-ray photoelectron spectroscopy (XPS) of the as-milled $NaBH_4-0.05TiF_3$ and $3NaBH_4-TiF_3$ samples after dehydrogenation was conducted using a SPECS PHOIBOS 100 Analyzer installed in a high-vacuum chamber with the base pressure below 10^{-8} mbar; X-ray excitation was provided by Al Kα radiation. The XPS binding energy spectra were recorded at the pass energy of 20 eV in the fixed analyzer transmission mode, and the XPS spectra of the doped samples were collected after bombardment of the sample using an Ar ion source with ion energy of 5 keV. Samples were prepared inside an Ar glovebox, by dusting powders onto an adhesive carbon tape. The samples were then placed in a sealed container to reduce oxidation during transportation from the glovebox to the XPS apparatus. The binding energy reference was taken as the main component of the C 1s peak at 284.5 eV. Analysis of the XPS data was carried out using the commercial CasaXPS2.3.15 software

package. The background was corrected using the linear approximation.

3. RESULTS AND DISCUSSION

3.1. Dehydrogenation Performance of $NaBH_4$ with Ti-Based Additives. The influence of the addition of titanium-based catalysts on the isothermal hydrogen desorption behavior of the $NaBH_4$ at 440 °C was qualitatively evaluated, as shown in Figure 1. It is apparent that the hydrogen desorption properties of $NaBH_4$ are slightly promoted by doping with Ti or TiH_2, but significantly improved by the addition of TiF_3. As shown in the figure, the ball-milled $NaBH_4$ sample only desorbed about 1.5 and 2.0 wt % hydrogen within 400 and 800 min, respectively. For the $NaBH_4$−0.05Ti sample, a hydrogen desorption capacity of 1.65 wt % was reached within 400 min. Furthermore, the sample can desorb 2.3 wt % hydrogen after a prolonged 800 min desorption. The $NaBH_4$−0.05TiH_2 sample showed an initial rate similar to that of the $NaBH_4$−0.05Ti sample, but ultimately showed a higher desorbed capacity, desorbing 1.85 wt % hydrogen within 400 min and 2.5 wt % hydrogen after 800 min. However, for the $NaBH_4$−0.05TiF_3 sample, a higher hydrogen desorption capacity of 3.2 and 3.95 wt % was obtained within 400 and 800 min, respectively, which are 1.7 and 1.95 wt % higher, respectively, than for the pristine $NaBH_4$ sample.

Although isothermal dehydrogenation studies are normally used to judge material performance characteristics such as storage capacity and kinetics at the desired temperature, temperature-programmed desorption (TPD) data provide an overall picture of the dehydrogenation process over a wide temperature range. Figure 2 compares the TPD profiles of the pristine $NaBH_4$ sample and those with the 5 mol % titanium-based catalysts. Evidently, the addition of titanium-based catalysts enhances the hydrogen desorption rate and increases the weight of hydrogen released from the $NaBH_4$, among which the best performance was obtained with the TiF_3-doped sample, where a reduction in the hydrogen desorption temperature was also observed. For example, the hydrogen release started at around 490 °C, and the weight loss was only 1.0 wt % after heating to 500 °C in the case of the pristine $NaBH_4$ sample. In contrast, the hydrogen released from the Ti-, TiH_2-, and TiF_3-doped $NaBH_4$ samples was increased to 1.79, 3.47, and 6.15 wt %, respectively, after heating to 500 °C. Interestingly, an apparent two-step dehydrogenation was observed in the case of $NaBH_4$−0.05TiF_3. The first step dehydrogenation started at around 300 °C and was completed at 360 °C, which may correspond to the reaction between the host $NaBH_4$ and the TiF_3 additive. A detailed analysis of the reaction mechanism between the $NaBH_4$ and the TiF_3 additive will be given in the following sections. Meanwhile, the onset temperature for the second dehydrogenation step of the $NaBH_4$−0.05TiF_3 sample is around 380 °C, which is about 110 °C lower than for the dehydrogenation of pure $NaBH_4$, indicating significant improvement in the dehydrogenation temperature. After 18 min at 500 °C, the dehydrogenation of the $NaBH_4$−0.05TiF_3 sample is completed, with 8.4 wt % hydrogen released as compared to 7.1, 6.0, and 4.0 wt % for the TiH_2-doped, Ti-doped, and pristine $NaBH_4$ samples, respectively. In contrast, the dehydrogenation of the Ti- and TiH_2-doped $NaBH_4$ samples is completed after 57 min at 500 °C. However, the hydrogen desorption process for pure $NaBH_4$ is still proceeding even after 107 min at 500 °C.

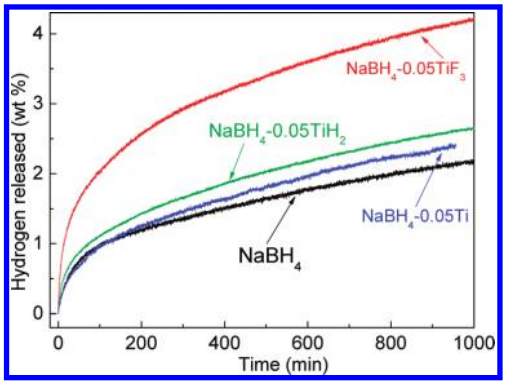

Figure 1. Isothermal dehydrogenation profiles of $NaBH_4$ with and without different titanium catalysts after ball milling in argon atmosphere for 2 h at 440 °C.

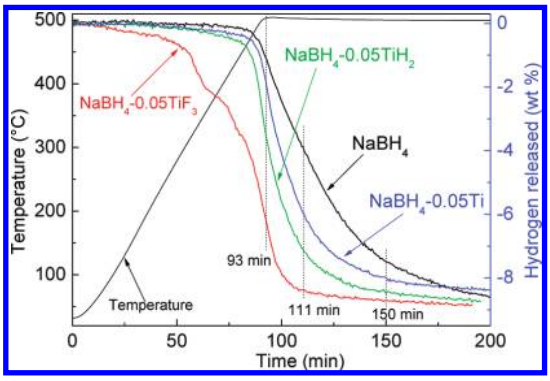

Figure 2. Temperature-programmed desorption (TPD) profiles of $NaBH_4$ with and without different titanium catalysts. The heating rate was 5 °C/min.

Combining the TPD and isothermal dehydrogenation results, it is clearly shown that the TiF_3 shows superior catalytic effects to either TiH_2 or Ti toward the dehydrogenation of $NaBH_4$. The observed enhancement of the decomposition of $NaBH_4$ is most likely induced by the catalytically active species that were formed in situ during the mechanical milling and/or heating processes. To understand the role of TiF_3, structural changes of the $NaBH_4$−0.05TiF_3 sample after ball milling (BM) and of the milled sample after dehydrogenation (De) at 500 °C (Figure 2) were investigated by means of XRD and FTIR. As can be seen in Figure 3a, the XRD pattern of the as-milled $NaBH_4$−0.05TiF_3 sample shows the presence of TiF_3 and $NaBH_4$, and no other phases can be detected, so that the sample shows the characteristics of a physical mixture of TiF_3 and $NaBH_4$ after 2 h of ball milling. However, after dehydrogenation at 500 °C, the TiF_3 and $NaBH_4$ peaks disappear, and new compounds, corresponding to Na, and NaF, were observed. The observation of metallic Na is attributed to the decomposition of $NaBH_4$. The absence of elemental boron from the dehydrogenation of TiF_3 catalyzed $NaBH_4$ can be explained by the fact that the boron phase in the dehydrogenated products of borohydrides is usually amorphous and therefore is hard to be identified by the XRD measurement. The formation of NaF indicates that the reaction of $NaBH_4$ and TiF_3 should take place during the dehydrogenation process, although no Ti-containing species could be detected in the dehydrogenation state.

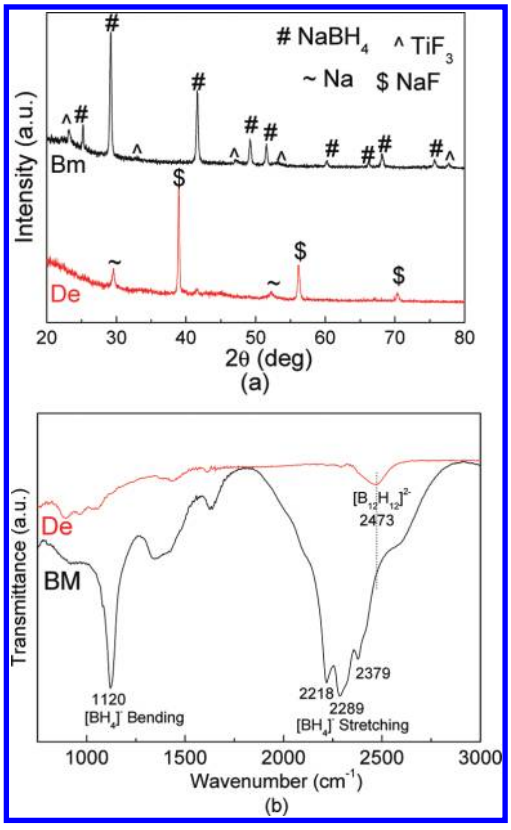

Figure 3. XRD patterns (a) and FTIR spectra (b) of the $NaBH_4$−0.05TiF_3 sample after 2 h ball milling (BM sample) and the ball milled sample after dehydrogenation at 500 °C (De sample).

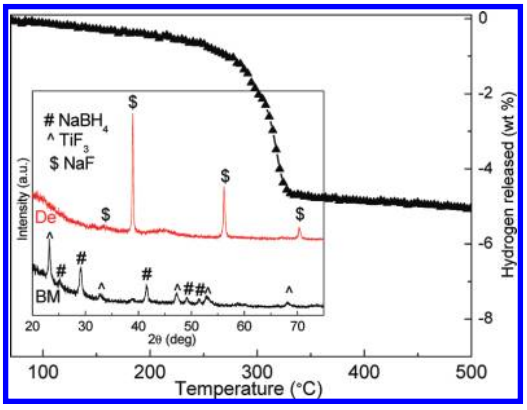

Figure 4. TPD profiles of 3$NaBH_4$−TiF_3 sample. The heating rate was 5 °C/min. The inset shows the XRD patterns of this 3$NaBH_4$−TiF_3 sample after 2 h ball milling (BM sample) and the ball milled sample after dehydrogenation at 500 °C (De sample).

The possible reactions during ball milling and dehydrogenation were further investigated by FTIR examination, as shown in Figure 3b. The results revealed the signatures of $[BH_4]^-$ bending at 1120 cm^{-1} and $[BH_4]^-$ stretching at 2218, 2289, and 2379 cm^{-1} in the spectra of the as-milled sample, which are located in the typical B−H vibration range of borohydride and are expected come from the $NaBH_4$. However, vibration of the B−H bonds from the $[BH_4]^-$ group disappeared after dehydrogenation, indicating the complete decomposition of $NaBH_4$. In addition, a new weak signal around 2473 cm^{-1} was also observed in the dehydrogenated state. The IR peak occurring at round 2500 cm^{-1} has also been seen by Muetterties et al.[45] when they studied the decomposition products of pure $LiBH_4$. Recent theoretical and experimental investigations have revealed that the discharge of hydrogen from $M(BH_4)_n$ (where M is metal) during the desorption process follows a multistep reaction, with $M_{2/n}B_{12}H_{12}$ as an intermediate species.[19,26,27,46−50] Therefore, this IR activity may possibly be due to trace amounts of $Na_2B_{12}H_{12}$, which is a very stable compound according to first-principles calculations,[25] although there was no direct observation of $Na_2B_{12}H_{12}$ formation in the XRD measurements due to the possible amorphous state.

For in-depth investigations on the reaction mechanism of TiF_3 and $NaBH_4$ and eliminating the possibility that the amount of TiF_3 addition was too low to generate any detectable diffraction intensity from the existing states of Ti in the TiF_3-doped sample, a larger amount of TiF_3 with mole ratio of 1:3 to $NaBH_4$ was prepared and examined. Figure 4 presents the TPD profiles of the 3$NaBH_4$−TiF_3 composite after 2 h of ball milling. The curve shows that the dehydrogenation starts from about 250 °C and ends at 330 °C. The dehydrogenation results are quite similar to the TPD results on $NaBH_4$−0.05TiF_3 (Figure 2), where that sample also displays its first dehydrogenation at around 300 °C, indicating that the first dehydrogenation in $NaBH_4$−0.05TiF_3 is mainly due to the reaction of TiF_3 with $NaBH_4$. The XRD patterns for the ball milled 3$NaBH_4$−TiF_3 sample, before and after dehydrogenation, are shown in the inset of Figure 4. Clearly, only $NaBH_4$ and TiF_3 were found in the as-milled sample, implying that the ball milling creates a physical mixture. After dehydrogenation, the $NaBH_4$ and TiF_3 peaks disappeared, and the new phase NaF was observed, but still no phases related to B or Ti can be identified, which is probably due to the presence of such species in a highly dispersed, nanocrystalline, and/or amorphous form.

It is known that XPS is a sensitive technique used for the determination of elemental and chemical composition of the surface of the investigated samples. Therefore, XPS measurements were carried out for identification of the states of the elements Ti and B present in the dehydrogenated TiF_3 added samples. Figure 5 shows the B1s and Ti2p photoemission peaks in the dehydrogenated $NaBH_4$−0.05TiF_3 and 3$NaBH_4$−TiF_3 samples. For the dehydrogenated $NaBH_4$−0.05TiF_3 sample, the B1s peak shows two different chemical states. The binding energies at 187.3 and 190.8 eV are quite similar to the binding energies of TiB_2 and B_xO_y ($1.5 < x/y < 3$), respectively, according to the literature.[51,52] Peak fitting reveals that the Ti 2p spectrum can be resolved into two sets of $2p_{3/2}$−$2p_{1/2}$ spin−orbit doublets at 453.8 and 460.0 eV, and 457.5 and 462.8 eV. The higher binding energy contribution (457.5 eV) is characteristic of TiO_x, whereas the second one (453.8 eV) can be attributed to TiB_2 according to the literature.[51−53] The appearance of reduced oxides (B_xO_y, TiO_x) may be due to oxidation in air when the sample was taken out from the glovebox and loaded to the XPS facility and the preferential sputtering of oxygen during the XPS measurement. Similar results (XPS shape and position) can be obtained for the dehydrogenated 3$NaBH_4$−TiF_3 sample, in which the B1s binding energies are 186.9 and 191.4 eV, Ti2p2/3 binding energies are 453.7 and 457.6 eV, and Ti2p1/2 binding energies are 459.9 and 463.4 eV. The results indicate that TiB_2 was formed during the reaction of TiF_3 with $NaBH_4$. A similar result has been reported for the $LiBH_4$−TiF_3 system, where TiB_2 compound was formed upon dehydrogenation.[13,51] On the other hand, the reaction pathway of $NaBH_4$ and TiF_3 can be estimated from

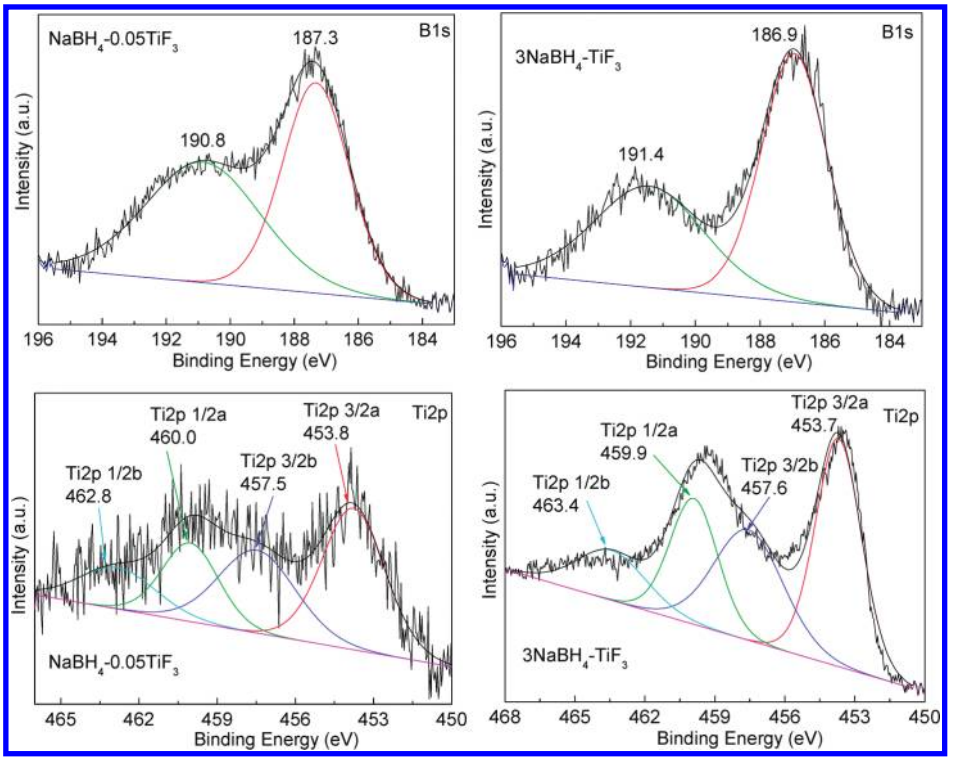

Figure 5. B1s and Ti2p XPS spectrum of the $NaBH_4-0.05TiF_3$ and $3NaBH_4-TiF_3$ samples after heating to 500 °C, respectively.

thermodynamics, in which HSC Chemistry program offers a very easy way to calculate the reaction enthalpy, entropy, Gibbs free energy, etc., as a function of temperature.[54] TiF_3 can react with $NaBH_4$, yielding titanium, titanium hydride, and titanium boride, respectively, according to the following reaction equations:[54]

$$3NaBH_4 + TiF_3 = 3NaF + Ti + 3B + 6H_2(g)$$
$$\Delta G = 96.181\ \text{kJ/mol} \quad (4)$$

$$3NaBH_4 + TiF_3 = 3NaF + TiH_2 + 3B + 5H_2(g)$$
$$\Delta G = -12.2\ \text{kJ/mol} \quad (5)$$

$$3NaBH_4 + TiF_3 = 3NaF + TiB_2 + B + 6H_2(g)$$
$$\Delta G = -179.5\ \text{kJ/mol} \quad (6)$$

From the viewpoint of thermodynamics, it can be seen that the formation of TiB_2 is favorable. On the basis of the XPS results and thermodynamic analysis, it can be concluded that TiF_3 will react with $NaBH_4$ to form NaF, TiB_2, and B during the heating process. Therefore, a simple mechanism can be proposed to explain the enhancement of the dehydrogenation of $NaBH_4-0.05TiF_3$. During the heating process, TiF_3 would first react with $NaBH_4$ as shown in reaction 6. As a result, TiB_2 was formed. During the subsequent heating, it acted as catalyst to promote the dehydrogenation of the remaining $NaBH_4$.

3.2. Rehydrogenation Performance of NaH+B Mixture with Ti-Based Additives. In our previous paper, we demonstrated the fact that the reversible dehydrogenation reactions of $NaBH_4$-based materials proceed in a liquid-phase environment provided by the molten Na, which probably affects the reversibility performance.[36,37] To avoid the effect of molten Na, the NaH+B samples with or without titanium-based catalysts were prepared through ball milling, and the hydrogenation properties of these samples were examined further. Figure 6a shows the XRD patterns of the NaH−B samples with and without catalyst doping after a 2 h ball milling. Clearly, in addition to the NaH phase, NaOH phase was also observed in all of the postmilled samples, which may originate from the oxidation of NaH. The absence of boron is attributed to the amorphous state. In addition, Ti and TiH_2 were also observed in the Ti and TiH_2 doped samples, respectively, indicating a physical mixture during ball milling. However, no Ti or F containing phases can be identified in the case of $NaH-B-0.05TiF_3$, which may due to the low concentration of TiF_3. Further FTIR examination showed that the signature Na−H vibration of NaH at 8822 cm^{-1} is observed in all of the samples (Figure 6b), indicating the presence of NaH in the postmilled samples. The peak at 1425 cm^{-1} belongs to the O−H bond, which is probably due to the presence of NaOH or air and moisture contamination during the measurement.[55]

The reversibility of these ball-milled samples was investigated under ~5.5 MPa of H_2 at 500 °C. Figure 7a displays the evolution of the composition and temperature versus time during the first rehydrogenation cycle of the four samples. The set temperature, ~500 °C, was reached in 40 min, and the total rehydrogenation was performed within around 10 h. All samples were found to be partially reversible under these conditions. It also can be seen that all of the samples started to absorb hydrogen after heating to about 450 °C. For the bare NaH+B sample, the hydrogen absorbed was only 0.58 wt % after heating to ~500 °C, which is lower than for $NaH-B-0.05Ti$ (0.86 wt %), $NaH-B-0.05TiH_2$ (0.77 wt %), and $NaH-B-0.05TiF_3$ (0.93 wt %). After 10 h at 500 °C, the hydrogenation of the bare NaH+B is still continuing, and a total of 1.88 wt % hydrogen could be absorbed. In contrast, the hydrogen absorbed was increased to 3.0, 3.1, and 4.0 wt % for the Ti, TiH_2, and TiF_3 doped NaH−B sample, respectively.

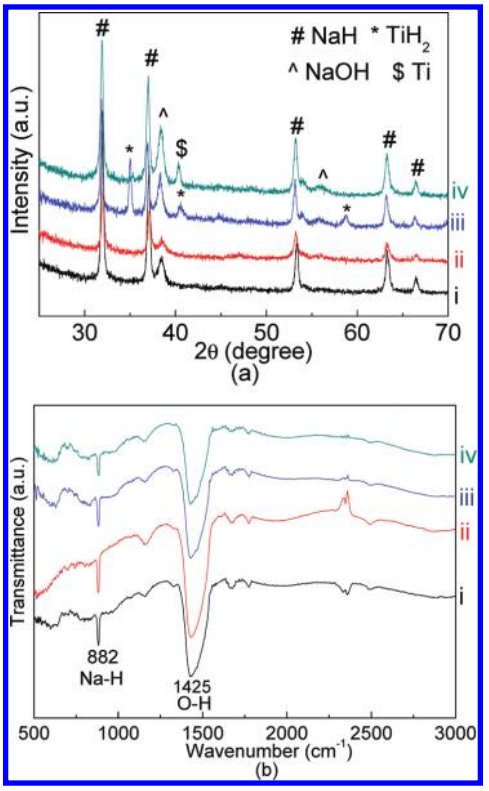

Figure 6. XRD patterns (a) and FTIR spectra (b) of the NaH−B (i), NaH−B−0.05TiF_3 (ii), NaH−B−0.05TiH_2 (iii), and NaH−B−0.05Ti (iv) samples after 2 h of ball milling.

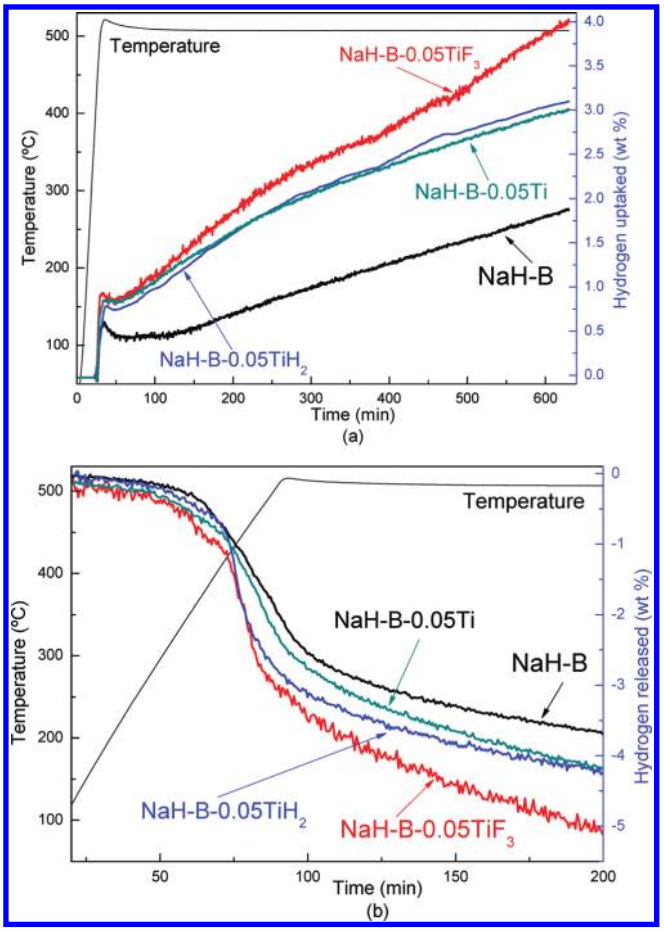

Figure 7. Hydrogenation (a) and dehydrogenation (b) profiles of the NaH+B mixture with and without different titanium catalysts.

Clearly, the rehydrogenation of NaH−B is improved by doping with titanium-based catalysts, and the best result is obtained from the TiF_3 doping.

The aforementioned rehydrogenation results are confirmed by the temperature-programmed desorption (TPD) curves. The TPD curves for the first dehydrogenation cycle of the pristine- and titanium-based catalyst doped samples are shown in Figure 7b. The first cycle reversible hydrogen capacity was 3.7 wt % for the undoped sample. However, the Ti- or TiH_2-doped samples could be rehydrogenated to 4.2 wt % in the first cycle, further confirming that the reversibility was slightly enhanced. Furthermore, the reversible hydrogen capacity for the TiF_3-doped samples was increased to 5.1 wt %, which is a little larger than for the NaH−B−0.05Ti or NaH−B−0.05TiH_2 sample, but much larger than that for the pristine sample. These results are in good agreement with the rehydrogenation measurements shown in Figure 7a and further confirm the effects of TiF_3 on the rehydrogenation properties of the pristine sample. It is also worth noting that the value from the TPD measurements is larger than the rehydrogenation value for the hydrogenated samples, which is due to the lack of complete reversibility for all of the samples, and, therefore, in addition to the rehydrogenated $NaBH_4$, there is still some NaH that will release hydrogen during the TPD measurement.

The rehydrogenated samples were then subjected to XRD and FTIR examination (Figure 8). From Figure 8a, in the XRD patterns of the rehydrogenation products of the pristine- and titanium-based additive doped NaH+B mixture, peaks corresponding to $NaBH_4$ can be clearly observed, although the intensity is not strong. Moreover, the NaH phase was still observed in the case of the pristine, as well as the Ti- and TiH_2-doped samples, but disappeared in the case of the TiF_3-doped sample. In contrast, the new peaks at 2θ of 38.4° and 55.3° correspond to the (200) and (220) peaks of NaF, respectively, but show a larger lattice parameter, which hints at the formation of $NaF_{1-x}H_x$, a reaction product of NaH and TiF_3, and can explain the absence of any NaH reflections (Table S1 in the Supporting Information). A similar phenomenon has been reported after mechanically milling NaH with TiF_3.[56] In addition to NaF or $NaF_{1-x}H_x$, NaH may react with TiF_3 to form TiH_2 according to $6NaH + 2TiF_3 = 6NaF + 2TiH_2 + H_2$ ($\Delta G = -607$ kJ/mol) or forming Ti according to $3NaH + TiF_3 = 3NaF + Ti + 1.5H_2$ ($\Delta G = -195$ kJ/mol).[54] From the thermodynamic point of view, the former reaction is more favorable. However, no Ti-containing species can be identified in the case of the TiF_3- or TiH_2-doped samples. In contrast, the formation of TiH_2 was observed in the case of the Ti-doped sample, which is due to the hydrogenation of Ti. The results indicate that TiH_2 may play a role in the hydrogenation of NaH+B samples with Ti-based additives doping. However, TiH_2 may interact with $NaBH_4$ to form TiB_2 when the system is dehydrogenated according to the report of Ti-based additives on the de-/rehydrogenation of LiH+MgB_2 mixture.[57] In addition, several unidentified peaks were observed in the pristine and Ti-based additives doped samples. They are probably attributable to the formation of B−O species, because a small amount of oxygen impurity (NaOH) is present in the starting material. For example, a bimetallic borohydride borate, $LiCa_3(BH_4)(BO_3)_2$, was discovered

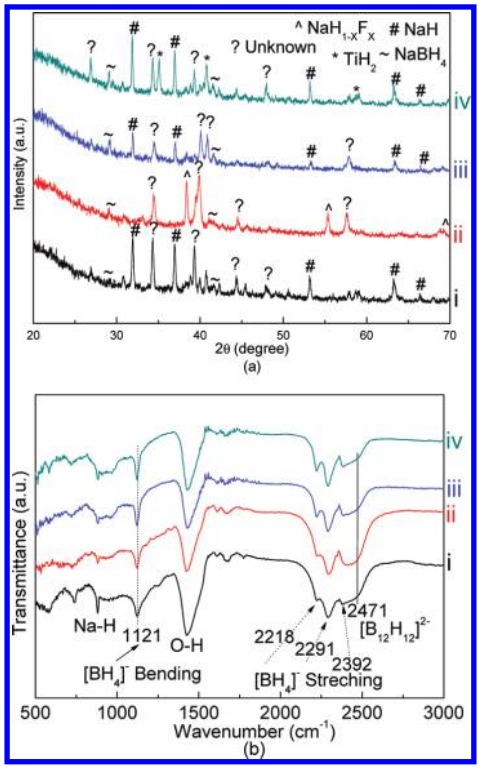

Figure 8. XRD patterns (a) and FTIR spectra (b) for the NaH−B (i), NaH−B−0.05TiF_3 (ii), NaH−B−0.05TiH_2 (iii), and NaH−B−0.05Ti (iv) samples after rehydrogenation.

during decomposition of $LiBH_4$−$Ca(BH_4)_2$−carbon composite if a small amount of oxygen impurity were present in the starting material or introduced during sample preparation.[58] The change in the structure during rehydrogenation was further investigated by FTIR examination, as shown in Figure 8b. The signatures of $[BH_4]^-$ bending at 1121 cm^{-1} and $[BH_4]^-$ stretching at 2218, 2291, and 2392 cm^{-1} were clearly revealed in the spectra of all of the rehydrogenated samples, indicating the recombination of $NaBH_4$. Meanwhile, the vibration of the Na−H bond was also observed, indicating the partial reversibility of $NaBH_4$, agreeing well with the XRD results (Figure 8a). In addition, a new transmittance emerges at around 2471 cm^{-1} that agrees well with the B−H vibration of $[B_{12}H_{12}]^{2-}$,[45] which may play a role in the partial reversibility observed in the $NaBH_4$ with and without catalyst doping.

4. DISCUSSION

It has been shown that the hydrogen storage performance of $NaBH_4$ was improved by introducing small amounts of Ti-based additives, including Ti, TiH_2, and TiF_3, among which the best performance was obtained in the case of doping with TiF_3. It is also proposed that both Ti^{3+} cations and F^- anions play important roles in the dehydrogenation process of the TiF_3-doped $NaBH_4$. In-depth investigations on the interaction of $NaBH_4$ with TiF_3 revealed that $NaBH_4$ was successfully destabilized by adding TiF_3. For example, the 3$NaBH_4$−TiF_3 sample can complete its dehydrogenation below 330 °C. However, the results shown above do not support the formation of $Ti(BH_4)_3$ during ball milling or the heating process. Therefore, the low dehydrogenation temperature is possibly due to the direct reaction of $NaBH_4$ and TiF_3 during the heating process. Thus, in the case of $NaBH_4$−0.05TiF_3, the TiF_3 will first react with $NaBH_4$ to form the active species TiB_2 and NaF, which play an important role in promoting the dehydrogenation of the unreacted $NaBH_4$. The catalyst particles formed in situ are usually nanosized and finely distributed in the hydride matrix, as shown for catalyst doped $LiBH_4$ by Pinkerton et al.,[59] resulting in good catalytic effects. Furthermore, due to the identical crystallographic structures of NaF and NaH,[42] the in situ formed NaF can work as a source of nucleation centers for the formation of NaH or Na, which promotes nucleation and growth upon dehydrogenation, and therefore accelerates the decomposition of $NaBH_4$.

It has also been shown that Ti-based additives Ti, TiH_2, and TiF_3 were all effectively to improve the hydrogen absorption behaviors of NaH+B mixture, among which the best performance was still obtained in the case of doping with TiF_3. The additive Ti in NaH+B will absorb hydrogen to generate TiH_2 during the hydrogenation process, which can be regarded as an effective additive in the system. For the TiF_3-doped NaH+B mixture, in addition to the possible formation of TiH_2, it was also indicated that the F anion can substitute for anionic H in NaH to form $NaF_{1-x}H_x$ during the hydrogenation process. Therefore, the observed promotion effect of TiF_3 on the reversible dehydrogenation of $NaBH_4$ should be understood as arising from the combined effects of active Ti and F containing species. They work together in the formation of TiH_2, and the substitution of the functional F anion F^- for H^-. All of these complex factors working together resulted in the improvement of the hydrogen storage performance of $NaBH_4$. However, TiH_2 may interact with $NaBH_4$ to form TiB_2 when the system is dehydrogenated. In this regard, TiB_2 will be the active Ti specie during the dehydrogenation/rehydrogenation cycling of TiF_3-doped $NaBH_4$ or NaH+B samples.

In addition, the presence of amorphous $Na_2B_{12}H_{12}$ product in the dehydrogenated states of TiF_3-doped $NaBH_4$ was confirmed by FTIR, which leads to a dehydrogenation capacity of $NaBH_4$ that is lower than the theoretical value (Figure 2). Actually, the amorphous $Na_2[B_{12}H_{12}]$ has been detected in the desorbed states of nanoconfined $NaBH_4$ and $NaBH_4$−MgH_2 composite.[26,27] However, the role of $B_{12}H_{12}$ could not be explained completely. Friedrichs et al. have proposed that the $Li_2B_{12}H_{12}$ formation in the desorption of $LiBH_4$ can be explained as a result of the reaction of diborane and $LiBH_4$.[49] This may also explain the formation of $[B_{12}H_{12}]_2$ species upon dehydrogenation in other borohydrides, because diborane may be released in the decomposition of borohydrides at high temperature (>400 °C). Furthermore, in our case, the presence of $Na_2B_{12}H_{12}$ was also observed in the rehydrogenated states of pure and Ti-doped NaH+B mixture, which may be one of the reasons for the only partial reversibility observed in the $NaBH_4$ with and without catalyst doping. Caputo et al. recently have calculated that $Na_2B_{12}H_{12}$ is very stable and therefore is not easily rehydrogenated to $NaBH_4$ under moderate conditions.[25] On the other hand, the general chemical inertness of boron and the phase separation will also lead to poor recombination kinetics.

Even though the dehydrogenation and rehydrogenation of $NaBH_4$ can be promoted by doping with TiF_3, the conditions required for dehydrogenation and hydrogenation are still too extreme for practical applications, and the reversible capacity for the whole system is low as well. However, the enhancement of dehydrogenation and rehydrogenation by doping with additives is a good indication of progress and gives encouragement for further study on this material.

5. CONCLUSION

The hydrogen de-/absorption properties of $NaBH_4$ (NaH+B) with different Ti-based additives, including Ti, TiH_2, and TiF_3, were investigated. TPD, isothermal dehydrogenation, XRD, XPS, and FTIR were employed to study the de-/rehydrogenation properties and characterize the de-/hydriding pathways and products. Hydrogen de-/absorption results revealed that among the different titanium-based additives, TiF_3 possessed the highest catalytic activity toward the hydrogen desorption and absorption reactions of $NaBH_4$. XRD and XPS results revealed that the TiF_3 reacts with $NaBH_4$ to form TiB_2 and NaF in the heating process. It was also revealed that the F anion can substitute for anionic H in NaH to form $NaF_{1-x}H_x$ during the hydrogenation process, which may play a role during hydrogenation. It was believed that the observed promotion effect of TiF_3 on the reversible dehydrogenation of $NaBH_4$ should be understood as arising from the combined effects of active Ti- and F-containing species. All of these complex factors working together resulted in improvement of the hydrogen storage performance of $NaBH_4$. FTIR spectroscopy also confirmed the presence of amorphous $Na_2B_{12}H_{12}$ product, in both the dehydrogenated and the rehydrogenated states, which may play a crucial role in the partial dehydrogenation and reversibility observed in the $NaBH_4$ with and without catalyst doping.

■ ASSOCIATED CONTENT

Supporting Information. Comparison of *d*-spacings for $NaH_{1-x}F_x$ with NaF and NaH. This material is available free of charge via the Internet at http://pubs.acs.org.

■ AUTHOR INFORMATION

Corresponding Author

*E-mail: jeff.mao@hotmail.com (J.M.), zguo@uow.edu.au (Z.G.).

■ ACKNOWLEDGMENT

We would like to acknowledge support from the University of Wollongong, as well as critical reading by Dr. Tania Silver.

■ REFERENCES

(1) Yang, J.; Sudik, A.; Wolverton, C.; Siegel, D. *J. Chem. Soc. Rev.* **2010**, *39*, 656.
(2) Schlapbach, L.; Züttel, A. *Nature* **2001**, *414*, 353.
(3) http://www1.eere.energy.gov/hydrogenandfuelcells/storage/pdfs/targets_onboard_hydro_storage_explanation.pdf (Web release date Jan 4, 2010).
(4) Urgnani, J.; Torres, F. J.; Palumbo, M.; Baricco, M. *Int. J. Hydrogen Energy* **2008**, *33*, 3111–3115.
(5) Martelli, P.; Caputo, R.; Remhof, A.; Mauron, P.; Borgschulte, A.; Züttel, A. *J. Phys. Chem. C* **2010**, *114*, 7173–7177.
(6) Zhang, Z. G.; Wang, H.; Zhu, M. *Int. J. Hydrogen Energy* **2011**, *36*, 8203.
(7) Züttel, A.; Rentsch, S.; Fischer, P.; Wenger, P.; Sudan, P.; Mauron, P.; Emmenegger, Ch. *J. Alloys Compd.* **2003**, *356*−*357*, 515–520.
(8) Mauron, P.; Buchter, F.; Friedrichs, O.; Remhof, A.; Bielmann, M.; Christoph, N. Z.; Züttel, A. *J. Phys. Chem. B* **2008**, *112*, 906–910.
(9) Mauron, P.; Bielmann, M.; Remhof, A.; Züttel, A.; Shim, J. H.; Cho, Y. W. *J. Phys. Chem. C* **2010**, *114*, 16801–16805.
(10) Pendolino, F.; Mauron, P.; Borgschulte, A.; Züttel, A. *J. Phys. Chem. C* **2009**, *113*, 17231–17234.
(11) Mao, J. F.; Guo, Z. P.; Liu, H. K.; Yu, X. B. *J. Alloys Compd.* **2009**, *487*, 434–438.
(12) Zhang, Y.; Zhang, W. S.; Wang, A. Q.; Sun, L. X.; Fan, M. Q.; Chu, H. L.; Sun, J. C.; Zhang, T. *Int. J. Hydrogen Energy* **2007**, *32*, 3976–3980.
(13) Zhang, Y.; Zhang, W. S.; Fan, M. Q.; Liu, S. S.; Chu, H. L.; Zhang, Y. H.; Gao, X. Y.; Sun, L. X. *J. Phys. Chem. C* **2008**, *112*, 4005–4010.
(14) Zhang, Y.; Tian, Q. F.; Chu, H. L.; Zhang, J.; Liu, S. S.; Sun, L. X. *J. Phys. Chem. C* **2009**, *113*, 18424–18430.
(15) Li, H. W.; Kikuchi, K.; Nakamori, Y.; Miwa, K.; Towata, S.; Orimo, S. *Scr. Mater.* **2007**, *57*, 679–682.
(16) Newhouse, R. J.; Stavila, V.; Hwang, S.-J.; Klebanoff, L. E.; Zhang, J. Z. *J. Phys. Chem. C* **2010**, *114*, 5224.
(17) Mao, J. F.; Guo, Z. P.; Poh, C. K.; Ranjbar, A.; Guo, Y. H.; Yu, X. B.; Liu, H. K. *J. Alloys Compd.* **2010**, *500*, 200–205.
(18) Minella, C. B.; Garroni, S.; Pistidda, C.; Gosalawit-Utke, R.; Barkhordarian, G.; Rongeat, C.; Lindemann, I.; Gutfleisch, O.; Jensen, T. R.; Cerenius, Y.; Christensen, J.; Baro, M. D.; Bormann, R.; Klassen, T.; Dornheim, M. *J. Phys. Chem. C* **2011**, *115*, 2497–2504.
(19) Minella, C. B.; Garroni, S.; Olid, D.; Teixidor, F.; Pistidda, C.; Lindemann, I.; Gutfleisch, O.; Baro, M. D.; Bormann, R.; Klassen, T.; Dornheim, M. *J. Phys. Chem. C* **2011**, *115*, 18010–18014.
(20) Orimo, S.; Nakamori, Y.; Eliseo, J. R.; Züttel, A.; Jensen, C. M. *Chem. Rev.* **2007**, *107*, 4111–4132.
(21) Schlesinger, H.; Brown, H.; Finholt, A.; Gilbreath, J.; Hoekstra, H.; Hyde, E. *J. Am. Chem. Soc.* **1953**, *75*, 215–9.
(22) Liu, B. H.; Li, Z. P. *J. Power Sources* **2009**, *187*, 291–297.
(23) Muir, S. S.; Yao, X. D. *Int. J. Hydrogen Energy* **2011**, *36*, 5983.
(24) U.S. Department of Energy Hydrogen Program. Go/no-go recommendation for sodium borohydride for on-board vehicular hydrogen storage. Available at: NREL, http://www1.eere.energy.gov/hydrogenandfuelcells/pdfs/42220.pdf; 2007. NREL/MP-150-42220.
(25) Caputo, R.; Garroni, S.; Olid, D.; Teixidor, F.; Surińach, S.; Dolors Baró, M. *Phys. Chem. Chem. Phys.* **2010**, *12*, 15093–15100.
(26) Garroni, S.; Milanese, C.; Pottmaier, D.; Mulas, G.; Nolis, P.; Girella, A.; Caputo, R.; Olid, D.; Teixdor, F.; Baricco, M.; Marini, A.; Suriñach, S.; Baró, M. D. *J. Phys. Chem. C* **2011**, *115*, 16664–16671.
(27) Ngene, P.; van den Berg, R.; Verkuijlen, M. H. W.; de Jong, K. P.; de Jongh, P. E. *Energy Environ. Sci.* **2011**, *4*, 4108–4115.
(28) Barkhordarian, G.; Klassen, T.; Dornheim, M.; Bormann, R. *J. Alloys Compd.* **2007**, *440*, L18–L21.
(29) Mao, J. F.; Yu, X. B.; Guo, Z. P.; Liu, H. K.; Wu, Z.; Ni, J. *J. Alloys Compd.* **2009**, *479*, 619.
(30) Garroni, S.; Pistidda, C.; Brunelli, M.; Vaughan, G. B. M.; Surinach, S.; Baró, M. D. *Scr. Mater.* **2009**, *60*, 1129.
(31) Pistidda, C.; Garroni, S.; Minella, C.; Dolci, F.; Jensen, T. R.; Nolis, P.; Bösenberg, U.; Cerenius, Y.; Lohstroh, W.; Fichtner, M.; Baró, M. D.; Bormann, R.; Dornheim, M. *J. Phys. Chem. C* **2010**, *114*, 21816–21823.
(32) Milanese, C.; Garroni, S.; Girella, A.; Mulas, G.; Berbenni, V.; Bruni, G.; Suriach, S.; Baró, M. D.; Marini, A. *J. Phys. Chem. C* **2011**, *115*, 3151–3162.
(33) Garroni, S.; Milanese, C.; Girella, A.; Marini, A.; Mulas, G.; Menéndez, E.; Pistidda, C.; Dornheim, M.; Suriñach, S.; Baró, M. D. *Int. J. Hydrogen Energy* **2010**, *35*, 5434.
(34) Pottmaier, D.; Pistidda, C.; Groppo, E.; Bordiga, S.; Spoto, G.; Dornheim, M.; Baricco, M. *Int. J. Hydrogen Energy* **2011**, *36*, 7891.
(35) Pistidda, C.; Barkhordarian, G.; Rzeszuteka, A.; Garroni, S.; Minella, C. B.; Baró, M. D.; Nolis, P.; Bormann, R.; Klassen, T.; Dornheim, M. *Scr. Mater.* **2011**, *64*, 1035.
(36) Mao, J. F.; Yu, X. B.; Guo, Z. P.; Poh, C. K.; Liu, H. K.; Wu, Z.; Ni, J. *J. Phys. Chem. C* **2009**, *113*, 10813.
(37) Mao, J. F.; Guo, Z. P.; Yu, X. B.; Liu, H. K. *J. Phys. Chem. C* **2011**, *115*, 9283–9290.
(38) Jin, S. A.; Shim, J. H.; Cho, Y. W.; Yi, K. W.; Zabara, O.; Fichtner, M. *Scr. Mater.* **2008**, *58*, 963–965.
(39) Ampoumogli, A.; Steriotis, T.; Trikalitis, P.; Giasafaki, D.; Bardaji, E. G.; Fichtner, M.; Charalambopoulou, G. *J. Alloys Compd.* **2011**, *509S*, S705–S708.

(40) Bogdanović, B.; Schwickardi, M. *J. Alloys Compd.* **1997**, *253*−*254*, 1.
(41) Yin, L. C.; Wang, P.; Kang, X. D.; Sun, C. H.; Cheng, H. M. *Phys. Chem. Chem. Phys.* **2007**, *9*, 1499.
(42) Liu, Y. F.; Wang, F. H.; Cao, Y. H.; Gao, M. X.; Pan, H. G.; Wang, Q. D. *Energy Environ. Sci.* **2010**, *3*, 645–653.
(43) Yin, L. C.; Wang, P.; Fang, Z. Z.; Cheng, H. M. *Chem. Phys. Lett.* **2008**, *450*, 318.
(44) Fang, Z. Z.; Kang, X. D.; Yang, Z. X.; Walker, G. S.; Wang, P. *J. Phys. Chem. C* **2011**, *115*, 11839–11845.
(45) Muetterties, E.; Merriefield, R.; Miller, H.; Knoth, W.; Downing, R. *J. Am. Chem. Soc.* **1962**, *84*, 2506.
(46) Ohba, N.; Miwa, K.; Aoki, M.; Noritake, T.; Towata, S.; Nakamori, Y.; Orimo, S.; Züttel, A. *Phys. Rev. B* **2006**, *74*, 075110.
(47) Ozolins, V.; Majzoub, E. H.; Wolverton, C. *J. Am. Chem. Soc.* **2009**, *131*, 230.
(48) Hwang, S. J.; Bowman, R. C., Jr.; Reiter, J. W.; Rijssenbeek, J.; Soloveichik, G. L.; Zhao, J.-C.; Kabbour, H.; Ahn, C. C. *J. Phys. Chem. C* **2008**, *112*, 3164.
(49) Friedrichs, O.; Remhof, A.; Hwang, S.-J.; Züttel, A. *Chem. Mater.* **2010**, *22*, 3265–3268.
(50) Yan, Y. G.; Li, H. W.; Hideki, M.; Miwa, K.; Towata, S. I.; Orimo, S. *J. Phys. Chem. C* **2011**, *115*, 19419–19423.
(51) Guo, Y. H.; Yu, X. B.; Gao, L.; Xia, G. L.; Guo, Z. P.; Liu, H. K. *Energy Environ. Sci.* **2010**, *3*, 465–470.
(52) Deprez, E.; Muñoz-Márquez, M. A.; Jimenez de Haro, M. C.; Palomares, F. J.; Soria, F.; Dornheim, M.; Bormann, R.; Fernández, A. *J. Appl. Phys.* **2011**, *109*, 014913.
(53) Sedona, F.; Rizzi, G. A.; Agnoli, S.; Llabrés i Xamena, F. X.; Papageorgiou, A.; Ostermann, D.; Sambi, M.; Finetti, P.; Schierbaum, K.; Granozzi, G. *J. Phys. Chem. B* **2005**, *109*, 24411–24426.
(54) Roine, A. Outokumpu HSC Chemistry for Windows: Chemical Reaction and Equilibrium Software with Extensive Thermodynamical Database, Version 5.1. 02103-ORC-T, Outokumpu Research Oy, Finland, 2002.
(55) Bukka, K.; Miller, J. D.; Shabtai, J. *Clays Clay Miner.* **1992**, *40*, 92.
(56) Majzoub, E. H.; Herberg, J. L.; Stumpf, R.; Spangler, S.; Maxwell, R. S. *J. Alloys Compd.* **2005**, *394*, 265.
(57) Zhang, Y.; Morin, F.; Huot, J. *Int. J. Hydrogen Energy* **2011**, *36*, 5425–5430.
(58) Lee, Y. S.; Filinchuk, Y.; Lee, H. S.; Suh, J. Y.; Kim, J. W.; Yu, J. S.; Cho, Y. W. *J. Phys. Chem. C* **2011**, *115*, 10298–10304.
(59) Pinkerton, F. E.; Meyer, M. S.; Meisner, G. P.; Baloph, M. P. *J. Alloys Compd.* **2007**, *433*, 282.